J. Chem. Sci. (2020) 132:6
https://doi.org/10.1007/s12039-019-1695-5

REGULAR ARTICLE

Core–shell-structured MnO_2@carbon spheres and nitrogen-doped activated carbon for asymmetric supercapacitors with enhanced energy density

JIE WEN[a], XIAOPING CHEN[a], MAOLIN HUANG[a], WEN YANG[b,*] and JIE DENG[c]
[a]College of Chemistry and Chemical Engineering, Oil and Gas Field Applied Chemistry Key Laboratory of Sichuan Province, Southwest Petroleum University, Chengdu 610500, Sichuan, China
[b]Department of Chemistry and Bioengineering, Guilin University of Technology, Guilin 541004, China
[c]College of Pharmacy and Biological Engineering, Chengdu University, Chengdu 610106, China
E-mail: yangwen167@glut.edu.cn

MS received 26 April 2019; revised 1 August 2019; accepted 9 August 2019

Abstract. Asymmetric supercapacitors have potential applications in renewable-energy technology owing to their remarkable electrochemical properties. A high-voltage asymmetric supercapacitor was developed based on a core–shell-structured MnO_2@carbon sphere composite (MnO_2@CS) as the cathode, nitrogen-doped activated carbon as the anode and a neutral aqueous Na_2SO_4 solution as the electrolyte. MnO_2@CS was successfully fabricated by hydrothermally growing MnO_2 on the surface of carbon spheres. A nitrogen-containing benzoxazine resin was adopted as a precursor to produce *in situ* nitrogen-doped activated carbon. Such an aqueous electrolyte-based asymmetric supercapacitor can be cycled reversibly in the high-voltage region of 0–1.9 V and exhibits a superior energy density of 8 Wh kg^{-1} at an ultrahigh power density of 9627 W kg^{-1} owing to the matching of MnO_2@CS and porous nitrogen-doped activated carbon. Moreover, the asymmetric supercapacitor presents acceptable cycling performance, with 74.4% retention after 1000 cycles at 1 A g^{-1}, and a charge–discharge efficiency of the electrode of almost 100%.

Keywords. MnO_2; hydrothermal method; nitrogen-doped activated carbon; asymmetric supercapacitor.

1. Introduction

Owing to the limited availability of fossil energy sources and the increasing importance of environmental issues, the use of alternative energies, such as solar, wind, and biomass, has received increasing attention all over the world.[1] Supercapacitors, which can be used as energy storage devices, are also becoming increasingly more popular. They offer the advantages of high energy and power densities, good reversibility, non-pollutant, fast charge/discharge speeds, and long cycle life.[2]

At present, the materials used in metal oxide electrodes mainly include ruthenium oxide, cobalt oxide, nickel nitrate, manganese dioxide (MnO_2), and vanadium oxide. Among them, manganese dioxide has the advantages of being non-pollutant, having a high theoretical specific capacitance (1370 F g^{-1}),[3] and having abundant raw materials. Moreover, it is easy to control the morphology and structure of MnO_2, and as such, it is a very promising supercapacitor cathode material. There are many preparation methods for MnO_2, such as the hydrothermal synthesis method,[4] coprecipitation method,[5] sol–gel method,[6] and solid-phase method.[7] MnO_2 prepared *via* the hydrothermal method generally exhibits high purity and good dispersion. Ma *et al.*,[3] successfully prepared a core–shell-structured electrode material using MnO_2 nanosheets grown on the surface of MnO_2 nanowires. Their test results showed that the specific capacitance of this core–shell-structured material could be as high as 153.8 F g^{-1} at a current density of up to 20 A g^{-1}. After 1000 cycles of their stability test, the electrode material retained 98.1% of its initial capacitance.

However, MnO_2 has the disadvantages of low conductivity, small specific surface area, and easy agglomeration. The conductivity, structural stability, and service life of MnO_2 can be improved by combining it with carbon materials. Zhu *et al.*,[8] prepared flake graphene and MnO_2 composites. These composites exhibited a specific capacitance of 170 F g^{-1} at a scanning rate of 10 Mv s^{-1},

*For correspondence

Published online: 19 December 2019

and their retention rate was 82% after 1000 cycles. Chou *et al.,*[9] chemically deposited MnO_2 nanowires onto carbon nanotubes (CNTs) to prepare composites. The results showed that the specific capacitance of the composites was 167.5 F g^{-1} at a current density of 77 mA g^{-1}. After 3000 cycles, the specific-capacitance retention rate was 88%.

Asymmetric supercapacitors consist of an assembly comprising an electrode that stores energy at a negative potential and another electrode that stores energy at a positive potential. This allows them to have a larger potential window and a higher energy density than symmetric supercapacitors. Carbon materials are currently the most widely used cathode material in asymmetric supercapacitors.[10] Wu *et al.,*[11] used MnO_2 nanowires and graphene composites as positive electrodes and graphene as negative electrodes to fabricate asymmetric supercapacitors. Their test results showed that, for a power density of 5000 W kg^{-1}, the energy density attained was 7 Wh kg^{-1}. Li *et al.,*[12] assembled mesoporous MnO_2 microspheres and activated carbon into asymmetric supercapacitors. Their test results showed that the power and energy densities attained at a current density of 4 A g^{-1} were 2197 W kg^{-1} and 12.8 Wh kg^{-1}, respectively. As the specific capacitance of carbon materials is relatively low, doping with nitrogen atoms can be performed to introduce pseudo-capacitance, thereby improving the wettability of the electrolyte and its conductivity and, in turn, improving the electrochemical performance of the carbon material.[13,14] Doping methods can be classified into two types: surface modification and *in situ* doping. Compared to surface modification, *in situ* doping can be used to more evenly incorporate nitrogen atoms into the internal structure of the carbon material. The resulting material is usually more stable under long-term cyclic charging and discharging and has higher capacitance.[15,16]

In this study, the hydrothermal synthesis method was used to prepare a core–shell-structured MnO_2@-CS composite (MnO_2 petal nanosheets grown on carbon sphere surfaces) as a cathode material; a nitrogen-containing benzoxazine resin was adopted as a precursor to produce nitrogen-doped activated carbon as an anode material. With these materials, an asymmetric supercapacitor with excellent performance and low cost was fabricated.

2. Experimental

2.1 *Reagents and instruments*

All the chemicals used were of analytical grade and were used as received. The main reagents used in the experiment were resorcinol ($C_2H_6O_2$), formaldehyde (CH_2O, 38%), ammonia water ($NH_3{\cdot}H_2O$, 26%), potassium permanganate ($KMnO_4$), manganese sulfate monohydrate ($MnSO_4{\cdot}H_2O$), and bisphenol A-type benzoxazine (Huntsman).

The main instruments used were a high-pressure reaction kettle (GSH-2L, Weihai Chemical Machinery Co., Ltd, China), a high-temperature sintering tube furnace (OTF-1200X, Hefei Kejing Materials Technology Co., Ltd, China), a thermogravimetric/differential thermal analyzer (TGA/SDTA851e, Mettler Toledo, Switzerland), a field-emission scanning electron microscope (FE-SEM, Zeiss SUPRA 55VP, Germany), an X-ray diffractometer (XRD, PANalytical X'Pert PRO MPD, Holland), an X-ray photoelectron spectrometer (XPS, Thermo Fisher Scientific Escalab 250Xi, United States), a Brunauer–Emmett–Teller (BET) surface area and porosity analyzer (V-Sorb 2800P, Gold APP Instruments Corporation, China), and an electrochemical workstation (Metrohm PGSTAT302 N, Switzerland).

2.2 *Preparation of electrode materials*

2.2a *Preparation of the cathode material*: Core–shell-structured composites were prepared to be used as the cathode material. Carbon spheres were initially prepared using phenolic resin polymer spheres *via* the extensional Stöber method reported by Choma *et al.*[17] The carbon spheres were steam-activated at 800 °C for 3 h at a steam rate of 3.5 g min^{-1}. The resulting sample was denoted as CS. Afterwards, the hydrothermal synthesis method was used to prepare MnO_2/CS composites, which was reported in our previous work.[18] An $MnSO_4$ aqueous solution (3 mmol, 0.12 mmol mL^{-1}) was added to the suspension of CS (0.1 g of CS, 4 mg mL^{-1}). After ultrasonic dispersion for 30 min, a $KMnO_4$ aqueous solution (15 mmol, 0.17 mmol mL^{-1}) was added to the above-mentioned solution and stirred. Then, the mixture was transferred to a hydrothermal reactor and maintained at 140 °C for 2 h. Finally, the obtained black product was washed with deionized water multiple times and dried at 100 °C for 12 h. The as-prepared composite was marked as MnO_2@CS. For comparison, samples synthesized using the same procedure without the addition of CS were assigned as MnO_2.

2.2b *Preparation of the anode material*: First, 20 g of bisphenol A-type benzoxazine was added to a 100 mL flask and maintained at 120 °C until it had completely melted under vacuum conditions. After stirring, the resulting product was laid over a prepared mold, which was then transferred to the curing oven. The cured sample was then crushed into powder. Finally, the prepared resin was carbonized and activated using the same procedure as used for the phenolic resin microspheres. The resulting nitrogen-doped activated-carbon samples were denoted as NC.

2.3 *Electrochemical measurements*

A working electrode was fabricated by mixing the active material (80 wt.%), acetylene black (15 wt.%), and polyvinylidene fluoride (PVDF, 5 wt.%) and then coating this mixture onto nickel foam current collectors with a diameter of 1 cm. The as-fabricated electrodes were then dried in an oven at 100 °C for 24 h. The electrodes were then immersed in a 1 M $NaSO_4$ electrolyte for 6 h. Non-woven fabric was used as a separator. An asymmetric supercapacitor was fabricated using the electrodes, the separator, and a battery pack. The electrochemical properties of the single electrode and the asymmetric supercapacitor were tested using three-electrode and two-electrode systems, respectively. Graphite was selected for the counter electrode and Hg/HgO was selected for the reference electrode.

3. Results and Discussion

3.1 *Thermogravimetric analysis*

The carbonization temperature of the benzoxazine precursor was determined *via* thermogravimetric analysis under a nitrogen atmosphere at a heating rate of 10 °C min^{-1}. The results are shown in Figure 1. The weightlessness of the precursor in the 20 °C–200 °C range was attributed to the loss of adsorbed water. In the 200 °C–300 °C range, the observed weightlessness was mainly due to a small amount of organic solvent that existed in the raw material. The weight of the precursor decreased dramatically from 300 °C onwards, mainly because of the continuous production of small molecular gas molecules (such as H_2, H_2O, CO and NH_3) resulting from the fracture of molecular chains of reactants.[19] From 600 °C onwards, an approximately steady state was reached, indicating that the decomposition was complete. The carbon residue rate was approximately 36.9%. On the other hand, the weight loss of phenolic resin mainly occurred in the range of 100 °C–700 °C, which could be attributed to the release of lightweight gases, such as CO and CO_2, owing to the decomposition of hydroxymethyl groups and the crossed network structure of the resin.[20] After 700 °C, the decomposition process reached completion, and the measured carbon residue rate was approximately 56%.

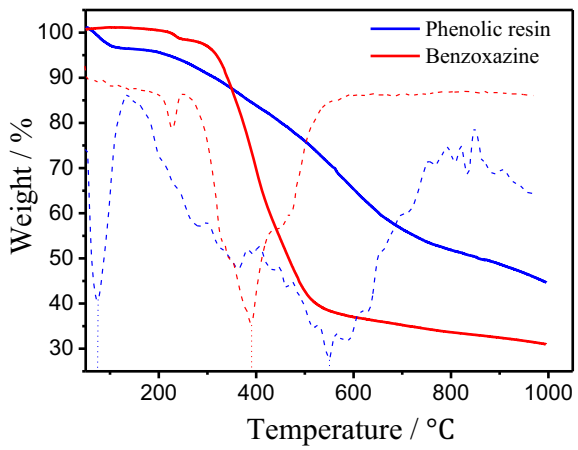

Figure 1. Thermal analysis curves for phenolic resin microspheres and benzoxazine. Solid and dashed lines represent thermogravimetric and differential thermogravimetric curves, respectively.

3.2 *Morphological analysis*

Morphological analysis was carried out *via* SEM. Figure 2a and 2b show SEM images of the phenolic resin spheres synthesized *via* the hydrothermal method after carbonization. The morphology of the prepared cathode material, MnO_2@CS, composites is shown in Figure 2c and 2d with different levels of magnification. The morphology of the anode material, NC, is shown in Figure 2e and 2f with different levels of magnification. It can be seen from Figure 2a and 2b that the microspheres had a uniform size and smooth surfaces. For the cathode material, shown in Figure 2c and 2d, a shell is formed on the surface of the microspheres. The exposed hollow part seen in some of the core–shell structures is caused by the falling off of the core due to the rupture of the shell. For the anode material derived from benzoxazine, small irregular particles of different sizes were obtained, as shown in Figure 2e and 2f. Abundant microporous structures could be formed on the material surface after steam activation, which allowed the electrode material to have a high specific surface area, which thus improved the specific capacitance of the supercapacitor.

3.3 *XRD analysis*

XRD analysis was performed to study the crystal properties and structures of the prepared materials. Figure 3 shows the XRD spectrum of the MnO_2@CS composites, which were synthesized via the hydrothermal method. It can be seen the CS sample exhibited only a very weak diffraction peak at 23°, whereas the MnO_2@CS sample exhibited four peaks at 12.3°, 24.8°, 36.6°, and 65.5° corresponding to the (003), (006), (101), and (110) reflections of the monoclinic δ-MnO_2 structure (JCPDS 86-0666), respectively.[21] Moreover, there were almost no impurity

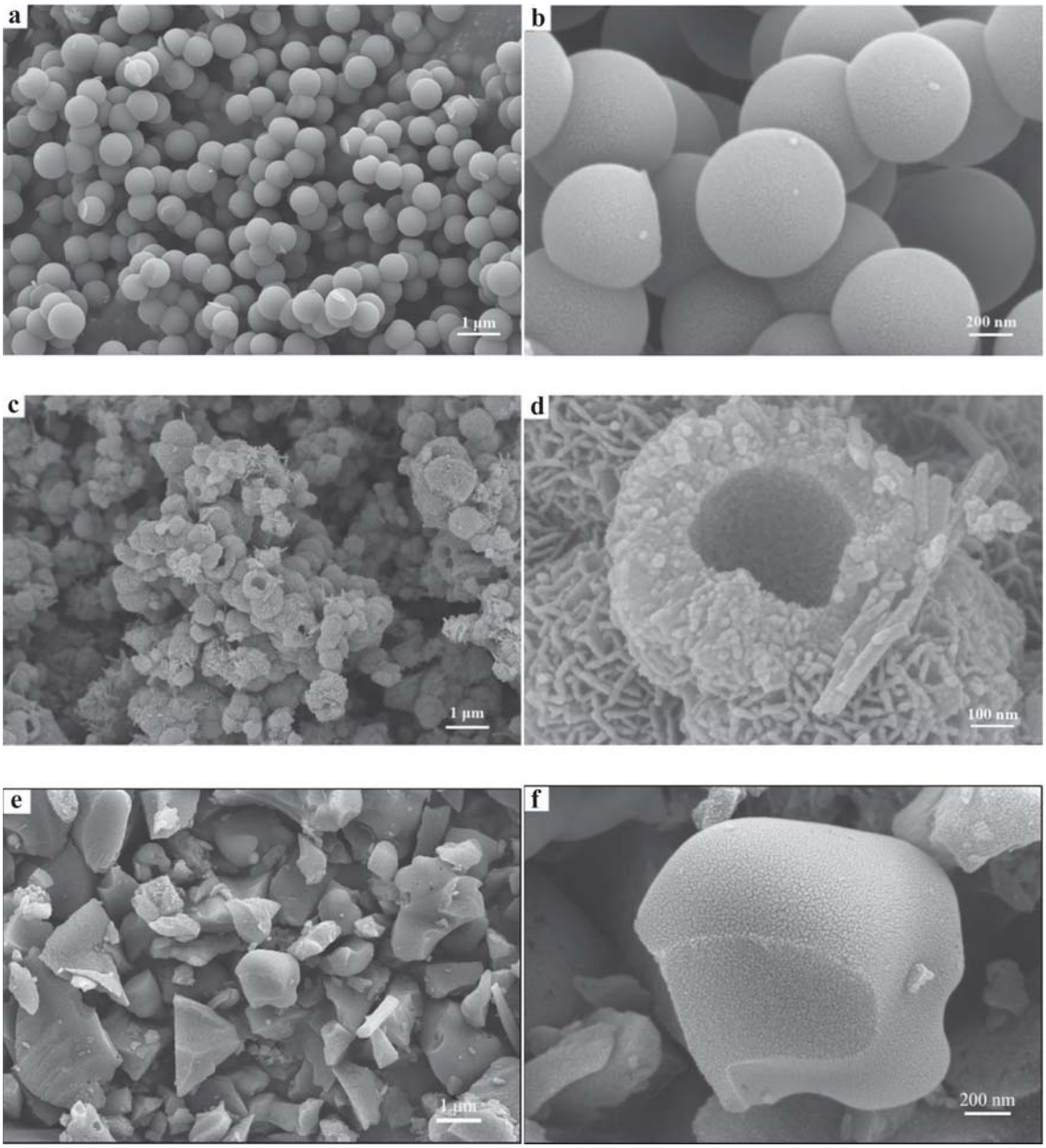

Figure 2. Scanning electron microscope (SEM) images of (a, b) carbon spheres after carbonization, (c, d) MnO_2@CS, and (e, f) NC.

peaks, indicating that both the crystallinity and purity of the MnO_2 in the composites was high.

3.4 *XPS analysis*

XPS analysis was carried out to verify the composition of the prepared materials. The wide-scan XPS spectrum of MnO_2@CS composite confirms the existence of C, O, and Mn (Figure 4a). The high-resolution spectrum of the O 1s band is presented in Figure 4b. The XPS peaks of 529.8 and 531.3 eV can be assigned to Mn–O–Mn and Mn–O–H, respectively.[22] The XPS results obtained for the anode material (NC) are shown in Figure 4c and 4d. Figure 4c shows that C, O, and N were the main elements on the material surface. For C1s, the characteristic peak was located at 284.8 eV, accounting for 85% of the total number of atoms on the surface. For O1s, the characteristic peak was located at 532.67 eV, accounting for 10% of the total number of atoms. For N1s, the characteristic peak was located at 401.29 eV, accounting for 5% of the total atomic number. Compared with anode materials made via other synthesis methods reported in the literature,[13,14,16] the benzoxazine-derived nitrogen-doped carbonaceous anode materials prepared in this study had a higher nitrogen content. Moreover, as can be

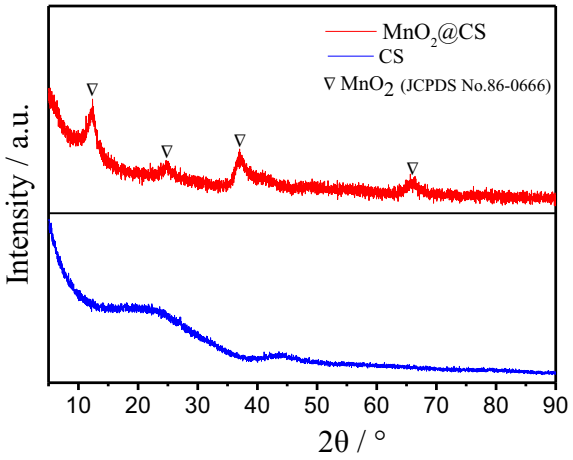

Figure 3. X-ray diffraction (XRD) patterns of the CS and MnO_2@CS samples.

seen from Figure 4d, the doping nitrogen atoms in the anode materials were mainly pyridine nitrogen (398.54 eV), pyrrole nitrogen (399.79 eV), and graphitic nitrogen (401.35 eV).[23,24]

3.5 *BET analysis*

Figure 5 illustrates the N_2 adsorption-desorption isotherms of the electrode materials, and the inset shows the measured pore size distribution. The isotherms for both MnO_2@CS and NC exhibited a type-I shape,[25] which indicates that these electrode materials were composed mainly of micropores. The textural parameters of the electrode materials calculated from the N_2 adsorption-desorption isotherms are given in Table 1. The specific surface area (S_{BET}) of NC reached 1306.4 $m^2\ g^{-1}$, which is higher than that of MnO_2@CS (970.3 $m^2\ g^{-1}$). Furthermore, the micropore volumes (V_{mic}) calculated via the Saito-Foley (SF) method for the NC and MnO_2@CS samples were 0.60 and 0.45 $cm^3\ g^{-1}$, respectively. The higher specific surface area of NC could be attributed to its more abundant micropores compared with MnO_2@CS. In addition, the total pore volume (V_t) of the NC and MnO_2@CS samples were 0.76 and 0.49 $cm^3\ g^{-1}$, respectively.

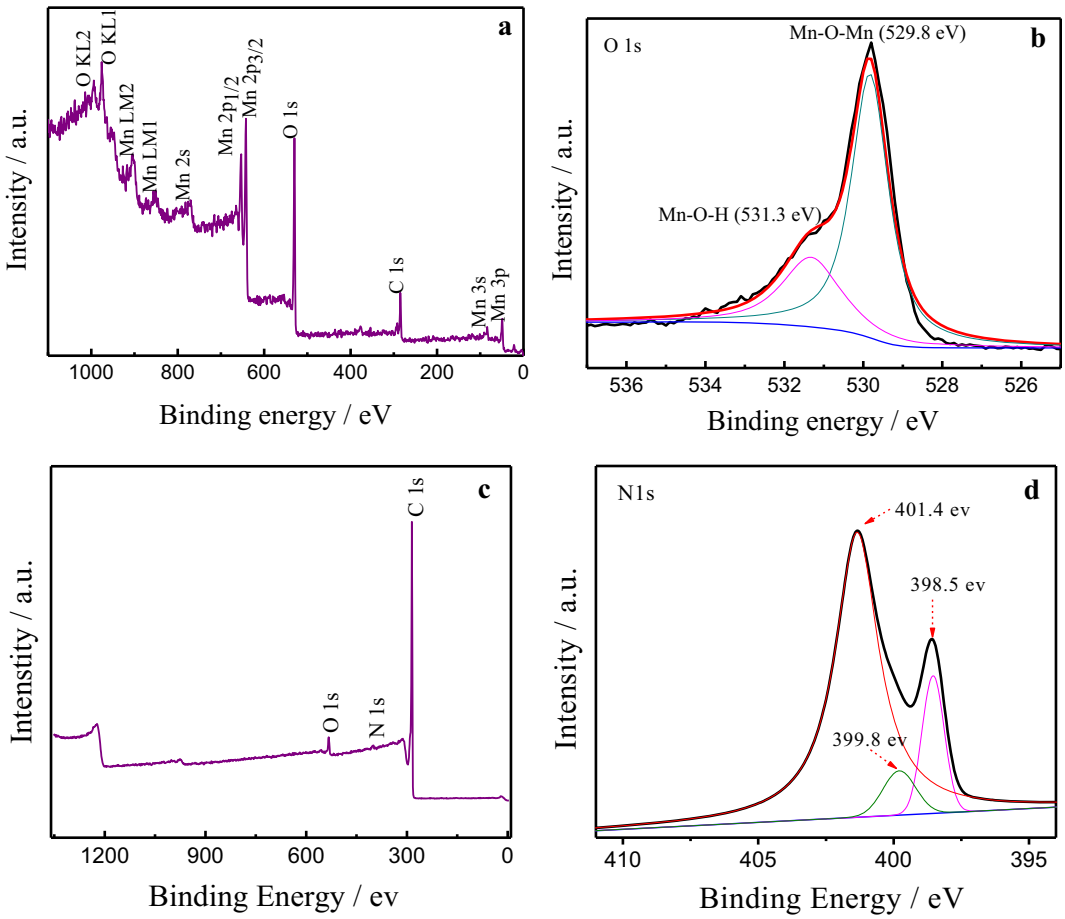

Figure 4. (a) X-ray photoelectron spectra (XPS) of the cathode material MnO_2@CS and (b) a close-up on the O1s peak. (c) XPS of the anode material NC and (d) a close-up on the N1s peak.

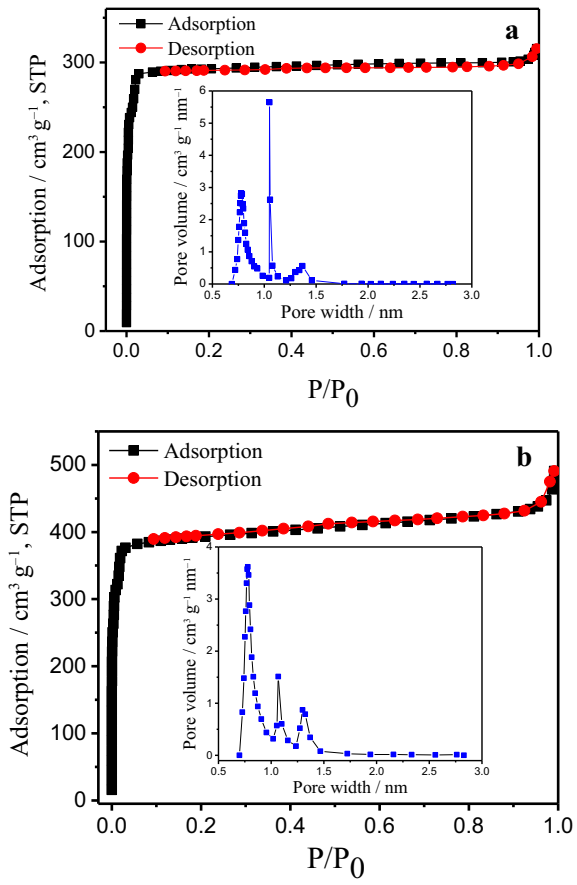

Figure 5. Nitrogen adsorption-desorption isotherms of (a) MnO_2@CS and (b) NC. Insets show corresponding pore size distributions.

3.6 *Electrochemical properties of electrode materials*

Cyclic voltammetry tests were carried out to analyze the electrochemical characteristics of the samples. Figure 6a shows the cyclic voltammograms (CVs) of CS, MnO_2, and MnO_2@CS measured at a scan rate of 10 mV s^{-1} in a 1 M Na_2SO_4 solution. The specific capacitances were calculated from the CV curves using Eq. 1:

$$SC = \frac{1}{m\upsilon\Delta V}\int I(V)\,dV \qquad (1)$$

where m (g) is the mass of the active material, υ (V s^{-1}) is the potential scan rate, ΔV (V) is the sweep potential window, and I (V) is the discharge current. The results show that the specific capacitances for CS, MnO_2, and MnO_2@CS were 141, 126, and 175 F g^{-1}, respectively. Thus, compared to the pure MnO_2 and CS, the composite material MnO_2@CS exhibited significantly improved capacitance. Furthermore, galvanostatic charge-discharge (GCD) tests were performed for MnO_2@CS for various current densities (i.e., 0.5, 1, 2, 5, and 10 A g^{-1}). As shown in Figure 6b, all the GCD curves exhibited an equilateral triangular shape, indicating good reversibility during the charge-discharge process. The specific capacitance (SC) could then be calculated according to Eq. 2:

$$C_S = \frac{I\Delta t}{m\Delta V} \qquad (2)$$

where C_s is the specific capacitance (F g^{-1}), I is the discharge current density (A g^{-1}), Δt is the time (s), ΔV indicates the voltage window (V), and m is the mass of the electrode (g). The calculated specific capacitance values for MnO_2@CS were 231, 206, 179, 160 and 124 F g^{-1} for current densities of 0.5, 1, 2, 5 and 10 A g^{-1}, respectively (Figure 6e). The specific capacitance values obtained were higher than those of other carbon-MnO_2 electrode materials reported in the literature, such as MG,[26] GHCS–MnO_2,[27] GW–MnO_2,[8] and MnO_2/CNTs.[28] Figure 6c and 6d shows CV curves of prepared NC under different scanning rates and GCD curves under different current densities, respectively. The shape of the curve in Figure 6c becomes more similar to a rectangle under large scanning rates, indicating that the material has good rate performance and is suitable for charging and discharging under a large current density. According to the GCD curves with different current densities, specific capacitances are calculated using Eq. 2. The results show that the specific capacitances are 189, 154, 138, 127 and 120 F g^{-1} at current densities of 0.5, 1, 2, 5 and 10 A g^{-1}, respectively (Figure 6e). Nyquist plots for MnO_2@CS and NC were obtained within an alternating current (AC) frequency range of 0.01–10,000 Hz and an open circuit potential, as shown in Figure 6f. The steep linear curve in the low-frequency region suggests nearly ideal capacitive performance. The intersection of the high-frequency region at the x-axis corresponds to the internal resistance (Re) of the electrode. Re is a critical parameter,

Table 1. Structural parameters of the MnO_2@CS composite and NC.

Sample	S_{BET} (m^2 g^{-1})	V_t (cm^3 g^{-1})	V_{mic} (cm^3 g^{-1})
MnO_2@CS	970.3	0.49	0.45
NC	1306.4	0.76	0.60

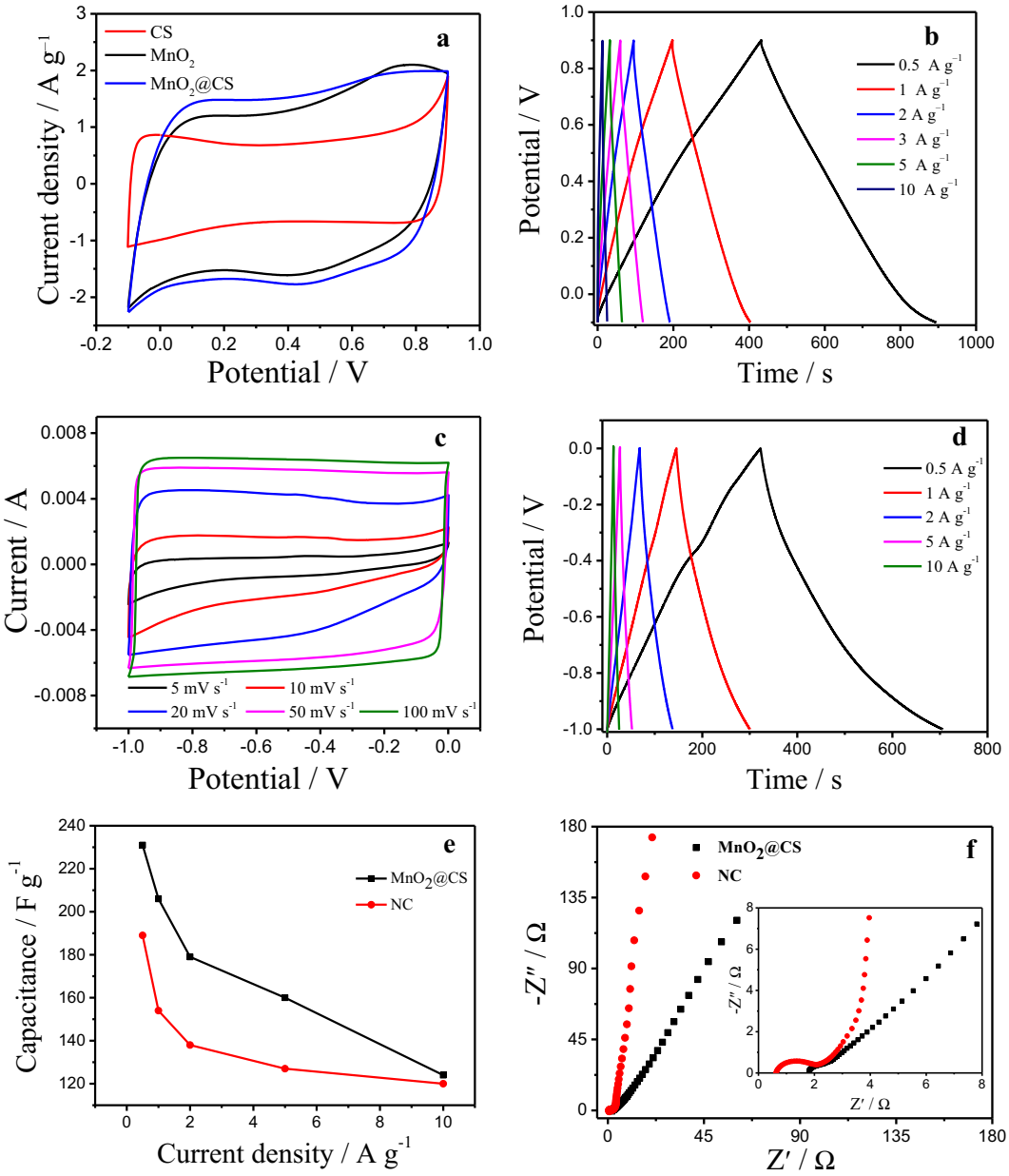

Figure 6. (a) Cyclic voltammograms of CS, MnO_2, and MnO_2@CS at a scanning rate of 10 mV s^{-1}. (b) Galvanostatic charge–discharge curves of MnO_2@CS for different current densities. (c) Cyclic voltammograms of NC at different scanning rates. (d) Galvanostatic charge–discharge curves of NC at different current densities. (e) Specific capacitance versus current density and (f) Nyquist plots of MnO_2@CS and NC.

which is affected by the current collector, binder, electrolyte and electrode spacer, and electrode material. The MnO_2@CS electrode displayed lower Re than did the NC electrode owing to the higher electron conductivity ability of the composite. In addition, the semi-circle in the high-frequency region indicates the charge transfer resistance (Rct). In the case of NC, the observation of semi-circles is mainly due to the doped redox heteroatoms or/and redox functional groups for faradic charge transfer processes. This further proves the successful doping of nitrogen.

3.7 *Electrochemical performances of the proposed asymmetric supercapacitor*

The performance of the fabricated asymmetric supercapacitor was first analyzed *via* cyclic voltammetry. Figure 7a shows the CVs of NC and MnO_2@CS measured at a scan rate of 10 mV s^{-1} in a 1 M Na_2SO_4 solution. It can be seen that the potential range of the NC electrode was from −1 to 0 V, whereas that of the MnO_2@CS was from −0.1 to 0.9 V. The shapes of both CV curves were similar to a rectangle, indicating

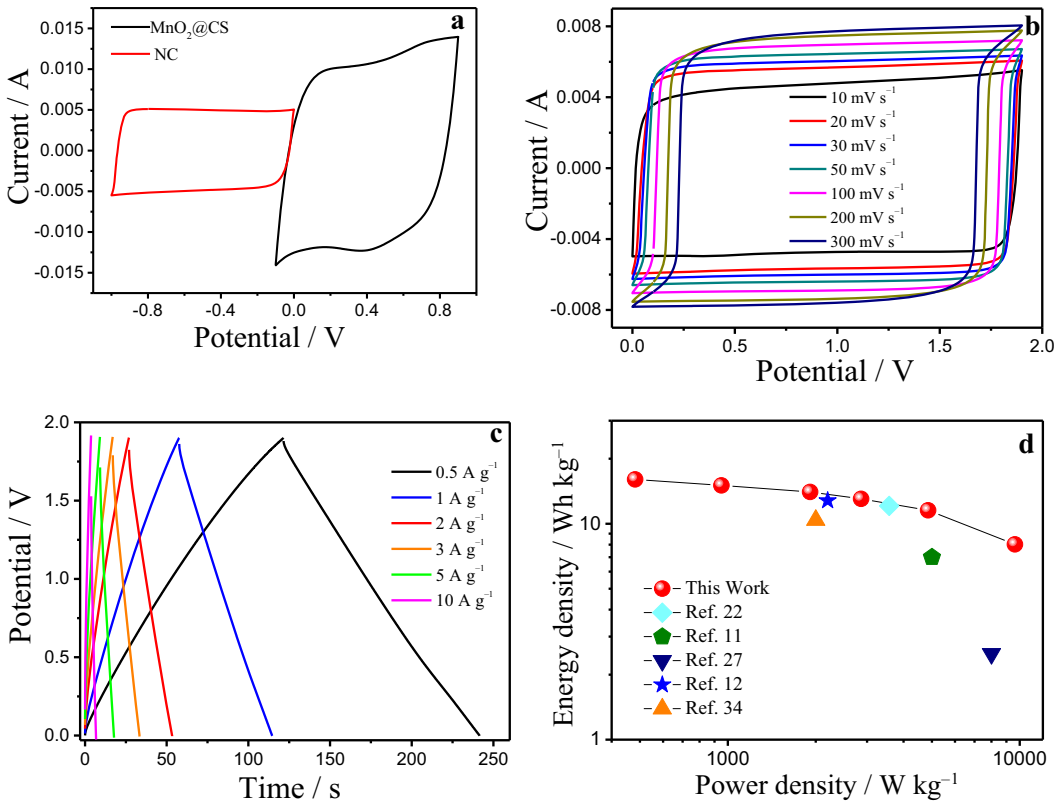

Figure 7. Cyclic voltammograms of (a) NC and MnO_2@CS at 10 mV s^{-1}; (b) MnO_2@CS//NC asymmetric supercapacitor at different scanning rates. (c) Galvanostatic charge–discharge curves of the MnO_2@CS//NC asymmetric supercapacitor at different current densities. (d) Ragone plot of MnO_2@CS//NC device.

that the materials yielded good supercapacitor properties in terms of electric double-layer capacitance. Among them, a pair of obvious redox peaks appeared in the CV curve of MnO_2@CS, which is believed to be the Faraday pseudocapacitance process of manganese oxide that originates from redox reactions between the different valence states of manganese.[29] The specific capacitances of the NC and MnO_2@CS electrodes were calculated using Eq. (1). The calculated results show that the specific capacitance of the NC electrode was 86 F g^{-1} and the specific capacitance of the MnO_2@CS electrode was 150 F g^{-1}. Considering the high specific capacitance of the MnO_2@CS composite and the fast ion transport characteristics of the NC material, NC was used as the anode material and MnO_2@CS was used as the cathode material to assemble an asymmetric supercapacitor. The mass ratio of the actual active substance can be calculated using Eq. (3):

$$\frac{m^-}{m^+} = \frac{C_{S^+}\Delta V_+}{C_{S^-}\Delta V_-} \tag{3}$$

where C_s (F g^{-1}) is the specific capacitance of a single electrode and ΔV (V) is the sweep potential window.[30] The anode and cathode materials were quite stable in the ranges from −1 to 0 V and from −0.1 to 0.9 V, respectively, and thus a wide potential window could be obtained by constructing an asymmetric supercapacitor. Figure 7b shows the cyclic voltammograms of the fabricated MnO_2@CS//NC asymmetric supercapacitor for different scan rates. It can be seen that, in the potential range of 0–1.9 V, a rectangular curve was obtained and there were no obvious redox peaks, indicating good electrical double-layer characteristics.[31] As the scanning rate increased, the capacitance of the asymmetric supercapacitor decreased, mainly because of the limited diffusion movement of Na^+ ions and protons at high scanning rates, which results in a low electrochemical utilization rate of active substances.

To further analyze the electrochemical performance of the fabricated MnO_2@CS//NC asymmetric supercapacitor, GCD tests were performed for various current densities. As shown in Figure 7c, in the potential range of 0–1.9 V, the GCD curves for different current densities exhibited an equilateral triangle shape and a good linear relationship between potential and time, indicating a fast I–V response and a small equivalent

series resistance, which is consistent with the obtained CV curves.[32] The calculated specific capacitance values of the fabricated asymmetrical supercapacitor were 32, 30, 28, 26, 23, and 16 F g^{-1} for current densities of 0.5, 1, 2, 3, 5, and 10 A g^{-1}, respectively. Using Eq. (4) and Eq. (5),[33] the energy density and the power density of asymmetric supercapacitors can be calculated, respectively; the calculated results are shown in Figure 7d:

$$E = \frac{1}{2} C \Delta V^2 \tag{4}$$

$$P = \frac{E}{\Delta t} \tag{5}$$

For an asymmetric supercapacitor with a power density of 2862 W kg^{-1}, the maximum energy density is 13 Wh kg^{-1}. Moreover, for a power density as high as 9627 W kg^{-1}, the energy density is still 8 Wh kg^{-1}. These results are comparable to, and in some cases significantly higher than, those of other MnO_2-based asymmetric supercapacitors reported in the literatures, such as MnO_2@CCNs//cross-linked carbon nanosheets (12.1 Wh kg^{-1} at a power density of 3570 W kg^{-1}),[22] MnO_2 nanowires–graphene composites//graphene (7 Wh kg^{-1} at a power density of 5000 W kg^{-1}),[11] carbon sphere//carbon sphere–MnO_2 composites (2.5 Wh kg^{-1} at a power density of 8000 W kg^{-1}),[27] mesoporous MnO_2 microspheres// activated carbon (12.8 Wh kg^{-1} at a power density of 2197 W kg^{-1}),[12] and ultrathin porous MnO_2 nanoflowers//functional mesoporous carbon nanotubes (10.4 Wh kg^{-1} at a power density of 2000 W kg^{-1}).[34]

3.8 *Cyclic stability of the fabricated asymmetric supercapacitor*

Long service life is an important requirement for supercapacitors.[35] For this reason, the fabricated asymmetric supercapacitor was subjected to 1000 galvanostatic charge–discharge cycles at a current density of 1 A g^{-1} to study the resulting changes in specific capacitance as well as the efficiency of the charge and discharge processes. The results are shown in Figure 8. After 1000 cycles, the specific capacitance retention rate was found to be 74.4%. This cycling stability is comparable to those of some other reported asymmetric supercapacitors, such as AC//MnO_2 in KOH (20% retention after 1500 cycles),[36] AC//α-MnO_2·nH_2O (93% retention after 100 cycles),[37] MWCNTs//MnO_2/MWCNT (72.3% retention after 300 cycles),[38] and MnO_2 nanowire/Graphene//Graphene

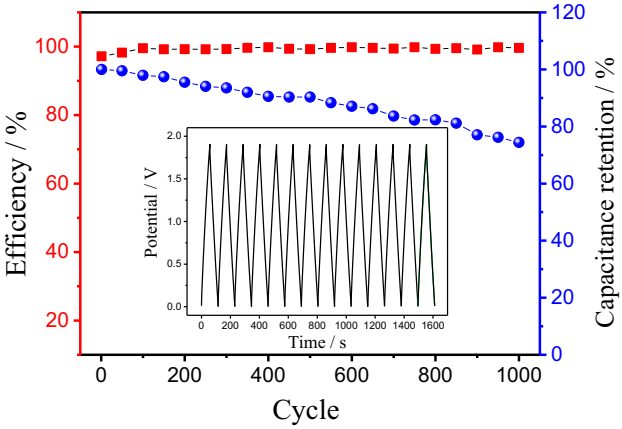

Figure 8. Charge–discharge efficiency and specific capacitance retention of the proposed MnO_2@CS//NC asymmetric supercapacitor at a current density of 1 A g^{-1}.

(79% retention after 1000 cycles).[11] Furthermore, it is noted that the charge–discharge efficiency of the supercapacitor was close to 100% except during the first several cycles. These results demonstrate that our device possesses good electrochemical stability.

4. Conclusions

A core–shell-structured MnO_2@CS composite was prepared by the hydrothermal method and used as the cathode material of an asymmetric supercapacitor; nitrogen-containing activated carbon (NC) produced from benzoxazine resin was used as the anode electrode. The results of our electrochemical performance tests show that the potential window of the proposed capacitor can reach 1.9 V. For a current density of 5 A g^{-1}, its energy and power densities can be as high as 8 Wh kg^{-1} and 9627 W kg^{-1}, respectively. After 1000 cycles, the specific capacitance retention rate of the asymmetric supercapacitor was found to be 74.4%. Removing the dissolved oxygen in the aqueous electrolyte and optimizing the mass ratio of the cathode and anode, volume ratio of the two electrodes, and ion concentration and pH value of the electrolyte are possible ways of improving the retention rate in the future.

Acknowledgements

This work was supported by the National Natural Science Foundation of China (No. 21206139).

References

1. Zhang Z, Yan Y, Zhang L, Chen Y and Ju S 2014 CFD investigation of CO_2 capture by methyldiethanolamine

and 2-(1-piperazinyl)-ethylamine in membranes: Effect of membrane properties *J. Nat. Gas Sci. Eng.* **19** 311
2. Zhu Y, Chu W, Wang N, Lin T, Yang W, Wen J and Zhao X S 2015 Self-assembled Ni/NiO/RGO heterostructures for high-performance supercapacitor *RSC Adv.* **5** 77958
3. Ma Z, Shao G, Fan Y, Wang G, Song J and Shen D 2016 Construction of Hierarchical α-MnO_2 Nanowires@Ultrathin δ- MnO_2 Nanosheets core-shell nanostructure with excellent cycling stability for high-power asymmetric supercapacitor electrodes *ACS Appl. Mater. Interf.* **8** 9050
4. Liu Y, Yan D, Zhuo R, Li S, Wu Z, Wang J, Ren P, Yan P and Geng Z 2013 Design, hydrothermal synthesis and electrochemical properties of porous birnessite-type manganese dioxide nanosheets on graphene as a hybrid material for supercapacitors *J. Power Sources* **242** 78
5. Lu X, Zou H, Zhang Y, Qiu H and Zheng Y 2015 Low-temperature selective catalytic reduction of NO over carbon nanotubes supported MnO_2 fabricated by co-precipitation method *Micro Nano Lett.* **10** 666
6. Sarkar A, Kumar S A, Kumar V and Kumar S 2015 Sol-gel synthesis of manganese oxide films and their predominant electrochemical properties *Electrochim. Acta* **167** 126
7. Tao J, Liu N, Ma W, Ding L, Li L, Su J and Gao Y 2013 Solid-state high performance flexible supercapacitors based on polypyrrole- MnO_2-carbon fiber hybrid structure *Sci. Rep.* **3** 1
8. Zhu J and He J 2012 Facile synthesis of graphene-wrapped honeycomb MnO_2 nanospheres and their application in supercapacitors *ACS Appl. Mater. Interf.* **4** 1770
9. Chou S L, Wang J Z, Chew S Y, Liu H K and Dou S X 2008 Electrodeposition of MnO_2 nanowires on carbon nanotube paper as free-standing, flexible electrode for supercapacitors *Electrochem. Commun.* **10** 1724
10. Wang J, Lu Y, Zhang N, Xiang X, Liang J and Chen J 2016 Ultrasmall SnS nanoparticles embedded in carbon spheres: A high-performance anode material for sodium ion batteries *RSC Adv.* **6** 95805
11. Wu Z S, Ren W, Wang D W, Li F, Liu B and Cheng H M 2011 High-energy MnO_2 nanowire/graphene and graphene asymmetric electrochemical capacitors *ACS Nano* **4** 5835
12. Li H, Zhang X, Ding R, Qi L and Wang H 2013 Facile synthesis of mesoporous MnO_2 microspheres for high performance AC//MnO_2 aqueous hybrid supercapacitors *Electrochim. Acta* **108** 497
13. Lee Y H, Lee Y F, Chang K H and Hu C C 2011 Synthesis of N-doped carbon nanosheets from collagen for electrochemical energy storage/conversion systems *Electrochem. Commun.* **13** 50
14. Jeong H M, Lee J W, Shin W H, Choi Y J, Shin H J, Kang J K and Choi J W 2011 Nitrogen-doped graphene for high-performance ultracapacitors and the importance of nitrogen-doped sites at basal planes *Nano Lett.* **11** 2472
15. Huang Z H, Liu T Y, Song Y, Li Y and Liu X X 2017 Balancing the electrical double layer capacitance and pseudocapacitance of hetero-atom doped carbon *Nanoscale* **9** 13119
16. Zhang Y, Ji L, Li W, Zhang Z, Lu L, Zhou L, Liu J, Chen Y, Liu L and Chen W 2016 Highly defective graphite for scalable synthesis of nitrogen doped holey graphene with high volumetric capacitance *J. Power Sources* **334** 104
17. Choma J, Jamioła D, Augustynek K, Marszewski M, Gao M and Jaroniec M 2012 New opportunities in Stöber synthesis: preparation of microporous and mesoporous carbon spheres *J. Mater. Chem.* **22** 12636
18. Chen X P, Wen J, Li Y T and Wang N 2018 Synthesis of core-shell structured MnO_2 petal nanosheet@carbon sphere composites and their application as supercapacitor electrodes *ChemistrySelect* **3** 9301
19. Wang M W, Ru J J and Lin C H 2016 The robustness of a thermoset of a main-chain type polybenzoxazine precursor prepared through a strategy of A–A and B–B polycondensation *RSC Adv.* **6** 18678
20. Yu J, Guo M, Muhammad F, Wang A, Yu G, Ma H and Zhu G 2014 Simple fabrication of an ordered nitrogen-doped mesoporous carbon with resorcinol–melamine–formaldehyde resin *Micropor. Mesopor. Mater.* **190** 117
21. Zhu H, Liu Q, Liu J, Li R, Zhang H, Hu S and Li Z 2015 Construction of porous hierarchical manganese dioxide on exfoliated titanium dioxide nanosheets as a novel electrode for supercapacitors *Electrochim. Acta* **178** 758
22. Li Y, Yu N, Yan P, Li Y, Zhou X, Chen S, Wang G, Wei T and Fan Z 2015 Fabrication of manganese dioxide nanoplates anchoring on biomass-derived cross-linked carbon nanosheets for high-performance asymmetric supercapacitors *J. Power Sources* **300** 309
23. Liu M, He S and Chen W 2014 Co_3O_4 nanowires supported on 3D N-doped carbon foam as an electrochemical sensing platform for efficient H_2O_2 detection *Nanoscale* **6** 11769
24. Zhong M, Song Y, Li Y, Ma C, Zhai X, Shi J, Guo Q and Liu L 2012 Effect of reduced graphene oxide on the properties of an activated carbon cloth/polyaniline flexible electrode for supercapacitor application *J. Power Sources* **217** 6
25. Duan X, Hu Z, Gao S, Shen R, Liu H, Chang J and Wang L 2018 Shale high pressure isothermal adsorption curve and the production dynamic experiments of gas well *Petrol. Explor. Dev.* **45** 127
26. Chu Q, Du J, Lu W, Chang G, Xing Z, Li H, Ge C, Lei W, Luo Y and Asiri A M 2012 Synthesis of a MnO_2 nanosheet/graphene flake composite and its application as a supercapacitor having high rate capability *Chempluschem* **77** 872
27. Lei Z, Zhang J and Zhao X S 2012 Ultrathin MnO_2 nanofibers grown on graphitic carbon spheres as high-performance asymmetric supercapacitor electrodes *J. Mater. Chem.* **22** 153
28. Li L, Hu Z A, An N, Yang Y Y, Li Z M and Wu H Y 2014 Facile synthesis of MnO_2/CNTs composite for supercapacitor electrodes with long cycle stability *J. Phys. Chem. C* **118** 22865
29. Peng L, Peng X, Liu B, Wu C, Xie Y and Yu G 2013 Ultrathin two-dimensional MnO_2/graphene hybrid

nanostructures for high-performance, flexible planar supercapacitors *Nano Lett.* **13** 2151
30. Sui L, Tang S, Dai Z, Zhu Z, Huangfu, H, Qin X, Deng Y and Haarberg G M 2015 Supercapacitive behavior of an asymmetric supercapacitor based on a $Ni(OH)_2$/XC-72 composite *New J. Chem*. **39** 9363
31. Fan Z, Yan J, Wei T, Zhi L, Ning G, Li T and Wei F 2011 Asymmetric supercapacitors based on graphene/MnO_2 and activated carbon nanofiber electrodes with high power and energy density *Adv. Funct. Mater*. **21** 2366
32. Qu Q, Zhang P, Wang B, Chen Y, Tian S, Wu Y and Holze R 2009 Electrochemical performance of MnO_2 nanorods in neutral aqueous electrolytes as a cathode for asymmetric supercapacitors *J. Phys. Chem. C* **113** 14020
33. Zhao Y, Ran W, He J, Huang Y, Liu Z, Liu W, Tang Y, Zhang L, Gao D and Gao F 2015 High-performance asymmetric supercapacitors based on multilayer MnO_2/graphene oxide nanoflakes and hierarchical porous carbon with enhanced cycling stability *Small* **11** 1310
34. Jiang H, Li C, Sun T and Ma J 2012 A green and high energy density asymmetric supercapacitor based on ultrathin MnO_2 nanostructures and functional mesoporous carbon nanotube electrodes *Nanoscale* **4** 807
35. Wang D W, Li F and Cheng H M 2008 Hierarchical porous nickel oxide and carbon as electrode materials for asymmetric supercapacitor *J. Power Sources* **185** 1563
36. Yuan A B and Zhang Q L 2006 A novel hybrid manganese dioxide/activated carbon supercapacitor using lithium hydroxide electrolyte *Electrochem. Comm.* **8** 1173
37. Hong M S, Lee S H and Kim S W 2002 Use of KCl aqueous electrolyte for 2 V manganese oxide/activated carbon hybrid capacitor *Electrochem. Solid-State Lett.* **5** 227
38. Wang G X, Zhang B L, Yu Z L and Qu M Z 2005 Manganese oxide/MWNTs composite electrodes for supercapacitors *Solid State Ionics* **176** 1169